

# Solute transport under oscillating electro-osmotic flow in a closed-ended cylindrical pore

Guy Z. Ramon 

Received: 31 December 2016 / Accepted: 12 December 2017 / Published online: 23 December 2017  
© Springer Science+Business Media B.V., part of Springer Nature 2017

**Abstract** Mass transfer in a closed-ended, cylindrical tube, under an oscillatory electro-osmotic flow, is theoretically studied. Analytical solutions are found for the distribution of the electric potential, the velocity field and the concentration field. The time-averaged mass flux is then calculated in terms of an effective diffusion coefficient, or dispersion coefficient, akin to the classical Taylor–Aris dispersion. Calculations suggest that enhancement of mass transfer in dead-end pores, modelled as a closed-ended cylindrical tube, should be possible using an AC electric field under acceptable operating conditions, allowing, for example, up to a threefold enhancement in pores with a radius of 1  $\mu\text{m}$ .

**Keywords** Electro-osmotic flow · Oscillations · Taylor–Aris dispersion

## 1 Introduction

Electro-osmotic flow (EOF) may be most simply described as the fluid motion resulting from an applied electric field acting on excess charges within an electrolyte solution. The formation of an electric double layer (EDL) at a charged solid surface creates a region with excess charge due to attraction and repulsion of co- and counter-ions, respectively [1]. In the presence of an electric field, the ions within the EDL migrate and viscously drag the adjacent fluid, resulting in bulk flow.

While microfluidic applications have been a major driver for studies aimed at exploiting EOFs and inducing mass-transfer enhancement on the microscale [2–6], other diffusion-limited processes may also benefit from such enhancement. Notably, adsorption and heterogeneous catalysis are often performed in packed bed reactors composed of pelletised porous substrates, in which inter-particle diffusive transport is often the rate-limiting step. Flow-induced mixing may be employed, to some extent, within the macroscale, inter-particle space, but is of limited effectiveness in the microscale pores within the pellets [7]. Other processes that suffer from similar shortcomings include various types of chromatographic separation [8] and super-capacitor electrodes [9]. This is particularly true inside dead-end pores—it is practically impossible to induce pressure-driven flow within such structures; hence, the potential advantage for EOF-mediated transport is clear, since these externally excited flows are possible even within such confined geometries.

---

Guy Z. Ramon (✉)

Department of Civil & Environmental Engineering, Technion-Israel Institute of Technology, Haifa 32000, Israel  
e-mail: ramong@technion.ac.il

The flow-field generated by an EOF in confined geometries has been reported in the literature. For example, EOF in closed-ended square and cylindrical channels has been presented by Marcos et al. [10, 11], who obtained analytical solutions for these problems, and by Zhang et al. [12] who compared an analytical solution to a numerical scheme. These studies have shown that the flow generated within the EDL, by the applied electric field, induces a pressure gradient which in turn drives a back-flow in the centre of the channel. However, the mass transfer under such conditions and, specifically, the time-averaged dispersion, was not considered. Huang and Lai [13] have presented an analytical study of the enhanced mass transfer in an oscillatory EOF, within a parallel-plate microchannel configuration. The characteristics of the enhanced dispersion follow similar trends to those observed for the pressure-driven case; however, the effect of the EDL thickness distinguishes between the two situations, as it influences the degree of non-uniformity exhibited by the velocity field. When the EDL is extremely thin, the velocity field approaches a plug-flow distribution, whence the dispersion coefficient diminishes substantially. However, under such conditions, it has been shown that mass-transfer enhancement is possible, if the solute undergoes a reversible exchange with the solid boundary [14].

However, for a closed-ended configuration, which may be representative of inter-particle conditions within granular beds and other microscale porous media, the possible effect of an EOF on mass transfer has not been studied. It is therefore the purpose of the present paper, to consider the mass transfer in AC-driven EOF, specifically, the time-averaged mass flux of an inert solute within a closed-ended tube. The paper is organised as follows: Sect. 2 contains the model derivation and obtained solutions for the velocity and concentration fields, as well as the dispersion coefficient; results are then presented and discussed in Sect. 3, with concluding remarks given in Sect. 4.

## 2 Model formulation

The model considers the axis-symmetric, fully developed velocity induced within a closed-ended tube by an external electric field applied along the axis, where  $z$  and  $r$  denote the axial and radial coordinates, respectively. The general features and notation follow similar lines to our earlier paper [14]. We begin by presenting the equations governing the velocity and concentration fields, followed by their solutions and, finally, the dispersion coefficient.

### 2.1 The electric field

The electro-osmotic flow problem requires a description of the electric body force resulting from the electric field acting within the EDL. For the case of a symmetric, monovalent electrolyte (such a NaCl), the electric potential is governed by the following Poisson–Boltzmann equation:

$$\frac{1}{r} \frac{d}{dr} \left( r \frac{d\psi}{dr} \right) = \frac{2n_0 e_0}{\epsilon} \sinh \left( \frac{e_0 \psi}{k_b T} \right), \quad (1)$$

where  $\psi$  denotes the electric potential,  $e_0$  is the elementary charge,  $n_0$  the bulk electrolyte concentration,  $T$  the absolute temperature,  $k_b$  the Boltzmann constant and  $\epsilon = \epsilon_0 \epsilon_r$  is the permittivity of the liquid medium, with  $\epsilon_0$  and  $\epsilon_r$  denoting the permittivity of vacuum and the relative permittivity of the liquid, respectively. Equation (1) is subject to the boundary conditions

$$\frac{d\psi}{dr} = 0, \quad r = 0, \quad (2a)$$

and

$$\psi = \psi_s, \quad r = R, \quad (2b)$$

in which  $\psi_s$  is equivalent to the zeta potential at the edge of the immobilised Stern layer, which is here assumed to be uniformly distributed on the solid boundary.

Equation (1) is non-linear and, generally, requires a numerical solution. However, we invoke the Debye–Hückel approximation,  $ze_0\psi \ll kT$ , so that  $\sinh(e_0\psi/kT) \simeq e_0\psi/kT$ , and Eq. (1) becomes, in scaled form,

$$\frac{1}{\eta} \frac{d}{d\eta} \left( \eta \frac{d\Psi}{d\eta} \right) = \lambda^2 \Psi. \quad (3)$$

Here,  $\eta = r/R$ ,  $\Psi = e_0\psi/kT$  is the scaled potential and  $\lambda = \chi R$  is the scaled reciprocal Debye length, where

$$\chi = \left( \frac{2e_0^2 n_0}{\epsilon kT} \right)^{1/2}, \quad (4)$$

is the inverse of the characteristic EDL thickness. Equation (3), has the boundary conditions

$$\frac{d\Psi}{d\eta} = 0, \quad \eta = 0, \quad (5a)$$

and

$$\Psi = \Psi_s, \quad \eta = 1. \quad (5b)$$

The solution to this boundary value problem may be written as

$$\Psi(\eta) = \Psi_s \frac{I_0(\lambda\eta)}{I_0(\lambda)}, \quad (6)$$

where  $I_0$  is the zeroth-order modified Bessel function of the first kind.

## 2.2 Velocity field

As previously shown [10–12], in a closed-ended pore, the EOF originating from within the EDL, will induce a pressure-driven back-flow in the centre of the pore. This is the consequence of mass conservation—while the liquid flows along the pore walls, the closed-end induces a higher pressure; further, at any cross-section, the net flow-rate will be zero as the EOF is balanced by the pressure-driven returning fluid. To find the velocity field, we write the equation of motion for an incompressible, fully developed, electrically driven flow in a cylindrical tube,

$$\rho \frac{\partial u}{\partial t} = \frac{\mu}{r} \frac{\partial}{\partial r} \left( r \frac{\partial u}{\partial r} \right) - \frac{\partial p}{\partial z} + \rho_e E, \quad (7)$$

where  $u$  is the axial velocity component,  $\mu$ ,  $\rho$ , are the fluid's viscosity and density, respectively and  $\rho_e$  is the charge density, such that the term  $\rho_e E$  represents the electric body force. Here, the boundary conditions are no-slip at the solid wall and a finite velocity at the tube axis

$$\frac{\partial u}{\partial r} = 0, \quad r = 0, \quad (8a)$$

and

$$u = 0, \quad r = R. \quad (8b)$$

The flow is assumed to be driven by a uniform, time-harmonic, electric field of the form

$$E(t) = E_0 e^{i\omega t}, \quad (9)$$

in which  $E_0$  is the amplitude of the applied electric field,  $i$  is the imaginary unit and  $\omega$  is the angular frequency of the oscillations. Since Eq. (7) is linear, we assume that the induced pressure gradient and velocity fields are also time-harmonic once the initial transient has decayed. The pressure gradient is then of the form

$$-\frac{\partial p}{\partial z} = K e^{i\omega t + \phi}, \quad (10)$$

where  $K$  is a measure of the amplitude of the resulting back-pressure gradient,  $\phi$  denotes the phase angle between the oscillating electric field and the induced back pressure, and the velocity is

$$u = \Re[U_s f(\eta) e^{i\omega t}], \quad (11)$$

with  $\Re[\cdot]$  the real part of a complex quantity. Here, the velocity scale is taken to be the Helmholtz–Smoluchowski velocity  $U_s = \epsilon \psi_s E_0 / \mu$ , which is the velocity reached at steady-state under a DC electric field of magnitude  $E_0$ . Under these assumptions and with the solution to the electric potential distribution, we have

$$i\alpha^2 f - \frac{1}{\eta} \frac{d}{d\eta} \left( \eta \frac{df}{d\eta} \right) = \tilde{K} + \lambda^2 \frac{I_0(\lambda\eta)}{I_0(\lambda)}, \quad (12)$$

where  $\tilde{K} = \rho K \tau / U_s$  is a scaled pressure gradient, with  $\tau = R^2 / \nu$  denoting the viscous time scale. This equation is subject to the boundary conditions

$$\frac{df}{dy} = 0, \quad \eta = 0, \quad (13a)$$

and

$$f = 1, \quad \eta = 1. \quad (13b)$$

The solution to Eq. (12) is

$$f = \frac{i\lambda^2}{\alpha^2 + i\lambda^2} \left( \frac{J_0(\hat{\alpha}\eta)}{J_0(\hat{\alpha})} - \frac{I_0(\lambda\eta)}{I_0(\lambda)} \right) - \frac{i\tilde{K}}{\alpha^2} \left( 1 - \frac{J_0(\hat{\alpha}\eta)}{J_0(\hat{\alpha})} \right), \quad (14)$$

where  $J_0$  is the zeroth-order Bessel function of the first kind,  $\hat{\alpha} \equiv i^{3/2}\alpha$ , with  $\alpha$  denoting the Womersley number, familiar from pressure-driven oscillating flow. We note that  $\alpha^2 \equiv R^2\omega/\nu$  is the ratio of the viscous time scale,  $R^2/\nu$  to the oscillation time scale,  $1/\omega$ . It is readily seen that this solution is a superposition of the AC-EOF obtained for an open-ended cylindrical tube, given by the first term, with a pressure-driven oscillatory flow, given by the second term. However, unlike the usual pressure-driven case, the pressure gradient is not a prescribed quantity; therefore,

an additional constraint is imposed on the flow, by requiring that the volumetric flow-rate at any cross-section be equal to zero, or

$$\int_0^1 u \eta \, d\eta = 0. \quad (15)$$

Performing the integration, the scaled amplitude of the induced pressure gradient is found to be

$$\tilde{K} = \frac{i\alpha^2 \lambda^2}{\lambda^2 + i\alpha^2} \frac{F_\lambda - F_\alpha}{1 - F_\alpha}, \quad (16)$$

with

$$F_\alpha = \frac{2 J_1(\hat{\alpha})}{\hat{\alpha} J_0(\hat{\alpha})}, \quad F_\lambda = \frac{2 J_1(\lambda)}{\lambda J_0(\lambda)}.$$

### 2.3 The concentration field

The concentration field of the soluble species is governed by an advection–diffusion equation

$$\frac{\partial C}{\partial t} + u \frac{\partial C}{\partial z} = D_m \left( \frac{1}{r} \frac{\partial}{\partial r} \left( r \frac{\partial C}{\partial r} \right) + \frac{\partial^2 C}{\partial z^2} \right), \quad (17)$$

where  $C$  is the concentration and  $D_m$  is the molecular diffusion coefficient. The boundary conditions are symmetry at the tube axis,

$$\frac{\partial c}{\partial r} = 0, \quad r = 0, \quad (18a)$$

and no-flux at the tube wall,

$$\frac{\partial C}{\partial r} = 0, \quad r = R. \quad (18b)$$

Neglecting end effects, we may seek a solution of the form [15, 16]

$$C(r, z, t) = \gamma \left( z + g(r) e^{i\omega t} \right), \quad (19)$$

in which the axial concentration gradient,  $\gamma$ , is assumed to be constant. The equation for the radial distribution of the solute is then, in non-dimensional form,

$$i\Omega^2 g - \frac{1}{\eta} \frac{d}{d\eta} \left( \eta \frac{dg}{d\eta} \right) = -\text{Pe} f, \quad (20)$$

where  $\text{Pe} = U_s R / D_m$  is the Péclet number,  $f$  is given by Eq. (14), and

$$\Omega^2 = \frac{R^2 \omega}{D_m} = \alpha^2 \text{Sc}, \quad (21)$$

is the ratio of the diffusive time scale to the oscillation time scale, with  $Sc = \nu/D$  denoting the Schmidt number. Equation (20) is subject to the boundary conditions

$$\frac{dg}{d\eta} = 0, \quad \eta = 0, \quad (22a)$$

and

$$\frac{dg}{d\eta} = 0, \quad \eta = 1, \quad (22b)$$

with the solution

$$g(\eta) = Pe \left( B_3 - B_1 \frac{I_0(\lambda\eta)}{I_0(\lambda)} + (B_4 - B_2) \frac{J_0(\hat{\alpha}\eta)}{J_0(\hat{\alpha})} + B_5 \frac{J_0(\hat{\Omega}\eta)}{J_0(\hat{\Omega})} \right), \quad (23)$$

where  $\hat{\Omega} = i^{3/2}\Omega$ , and the following definitions have been made:

$$B_1 = \frac{\lambda^2}{(\lambda^2 - i\alpha^2)(\lambda^2 - i\Omega^2)},$$

$$B_2 = \frac{i\lambda^2}{(\lambda^2 - i\alpha^2)(\alpha^2 - \Omega^2)},$$

$$B_3 = \frac{\tilde{K}}{\alpha^2\Omega^2}, \quad B_4 = \frac{\tilde{K}}{\alpha^2(\alpha^2 - \Omega^2)},$$

and

$$B_5 = B_2 \frac{G_\alpha}{\hat{\Omega}} \left( \frac{\tilde{K}(\alpha^2 + i\lambda^2)}{\alpha^2\lambda^2} \right) - B_1 \frac{G_\lambda}{\hat{\Omega}},$$

with

$$G_\lambda = \lambda \frac{J_1(\lambda)}{J_0(\lambda)}, \quad G_\alpha = \hat{\alpha} \frac{J_1(\hat{\alpha})}{J_0(\hat{\alpha})}, \quad G_\Omega = \hat{\Omega} \frac{J_1(\hat{\Omega})}{J_0(\hat{\Omega})}.$$

#### 2.4 The time-averaged streaming mass flux

With the velocity and concentration distributions obtained, we are in a position to calculate the time-averaged mass flux resulting from the interaction of the two oscillating fields. This may most conveniently be written as an enhanced diffusion or hydrodynamic dispersion coefficient,

$$D_e = -\frac{1}{2} \Re [\langle u^* g \rangle], \quad (24)$$

where angle brackets are a cross-sectional average, and the star denotes a complex conjugate. In scaled form, the ratio of the dispersion coefficient to the molecular diffusion coefficient may be expressed as [16, 17]

$$\frac{D_e}{D_m} = 1 - \frac{Pe}{2} \Re [\langle f^* g \rangle], \quad (25)$$

enabling one to easily appreciate the comparative contribution of the oscillation-induced transport. Substituting the expressions for the functions  $f$  and  $g$  and performing the necessary integration, we find the dispersion coefficient, which may be written, after some algebra, as

$$\begin{aligned}
 D_e = \text{Pe} \Re \left[ \frac{i\tilde{K}^*}{\alpha^2} \left( B_1 \left( H_{\lambda\alpha^*} - \frac{G_\alpha}{\hat{\alpha}^2} \right) + B_2 \left( H_\alpha - \frac{G_\alpha}{\hat{\alpha}^2} \right) + B_4 \left( \frac{1}{2} - \frac{G_\alpha}{\hat{\alpha}^2} \right) \right. \right. \\
 \left. \left. + B_5 \left( \frac{G_\alpha}{\hat{\alpha}^2} - H_{\alpha^*} \right) + B_6 \left( \frac{1}{\hat{\Omega}} + H_{\Omega\alpha^*} \right) \right) \right. \\
 - \frac{\lambda^2}{\lambda^2 + i\alpha^2} \left( B_1 (G + H_{\lambda\alpha}) + B_2 (H_{\alpha\lambda} + H_{\alpha^*}) \right) \\
 - B_4 \left( \frac{G_\alpha^*}{\hat{\alpha}^2} - \frac{G_\lambda}{\lambda^2} \right) - B_5 (H_{\alpha^*} - H_{\alpha\lambda}) \\
 \left. \left. + B_6 (H_{\Omega\lambda} + H_{\alpha^*\Omega}) \right) \right], \tag{26}
 \end{aligned}$$

where, for brevity, we introduce the notation

$$\begin{aligned}
 G &= \frac{1}{2} \left( 1 - \frac{I_1^2(\lambda)}{I_0^2(\lambda)} \right), \\
 H_{\alpha^*} &= \frac{G_\alpha - G_{\alpha^*}}{\hat{\alpha}^2 - \hat{\alpha}^{*2}}, \quad H_{\alpha\lambda} = \frac{G_\alpha + G_\lambda}{\hat{\alpha}^2 + \lambda^2}, \\
 H_{\lambda\alpha} &= \frac{G_\alpha + G_\lambda}{\lambda^2 + \hat{\alpha}^{*2}}, \quad H_{\lambda\alpha^*} = \frac{G_\lambda + G_{\alpha^*}}{\lambda^2 + \hat{\alpha}^{*2}},
 \end{aligned}$$

and

$$\begin{aligned}
 H_{\Omega\lambda} &= \frac{\hat{\Omega}}{\hat{\Omega}^2 - \hat{\alpha}^{*2}} \left( 1 - \frac{G_\lambda}{G_\Omega} \right), \\
 H_{\alpha^*\Omega} &= \frac{\hat{\Omega}}{\hat{\Omega}^2 - \hat{\alpha}^{*2}} \left( 1 - \frac{G_\alpha^*}{G_\Omega} \right), \\
 H_{\Omega\alpha^*} &= \frac{\hat{\Omega}}{\hat{\alpha}^{*2} - \hat{\Omega}^2} \left( 1 + \frac{G_\lambda}{G_\Omega} \right).
 \end{aligned}$$

### 3 Results and discussion

In the following section, calculations of the electric potential, velocity and concentration distribution are presented, as well as the resulting dispersion coefficient, as influenced by the dimensionless variables  $\alpha$ , representing the scaled oscillation frequency;  $\lambda$ , the EDL characteristic thickness;  $Sc$ , a measure of the solution transport properties, and the fluid motion, represented by  $Pe$ .

When applying an electric field to drive the EOF, a relatively wide range of frequencies is accessible provided that these are kept below  $\sim 1$  MHz, in order to avoid EDL relaxation effects. Further, the amplitude of the applied electric field must in general be  $E_0 < 100$  V/mm to avoid Joule heating and possible electro-kinetic instabilities [13]. These restrictions correspond with a range of scaled frequencies  $\alpha$ , e.g. in an aqueous solution with  $\nu \approx 10^{-6}$  m<sup>2</sup>/s, a value of  $\alpha = 0.5$  corresponds with a frequency of  $\sim 4$  Hz in a tube with  $R = 100$   $\mu$ m, while for a pore with  $R = 1$   $\mu$ m, a frequency of 1600 Hz corresponds with a value of  $\alpha \approx 0.1$ . To conform with the restricted amplitude, in an aqueous solution at  $T = 298$  K with  $\psi_s = -0.1$  V and  $Sc = 1000$ , we limit the velocity to  $U_s < 2$  mm/s, or  $Pe = 0.8 - 20$ , in pores of radii  $R = 0.1 - 10$   $\mu$ m, respectively.

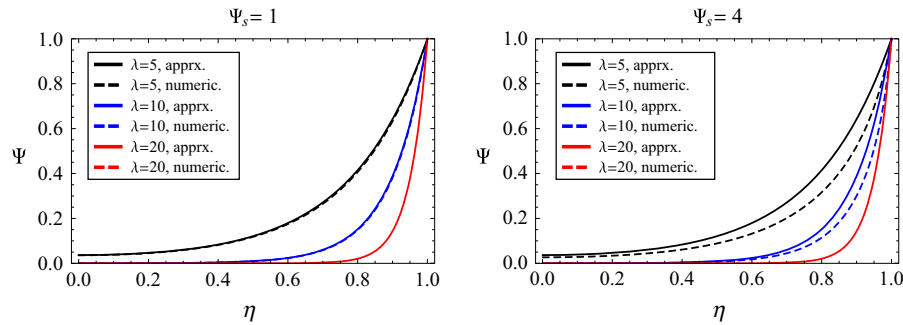


**Fig. 1** Distribution of the scaled electric potential,  $\Psi$ , in the electric double layer, calculated for various values of the parameter  $\lambda$ . Solid curves are calculations based on a numerical solution of the Poisson–Boltzmann equation, while dashed curves are calculated using the approximate analytical solution of the linearised equation

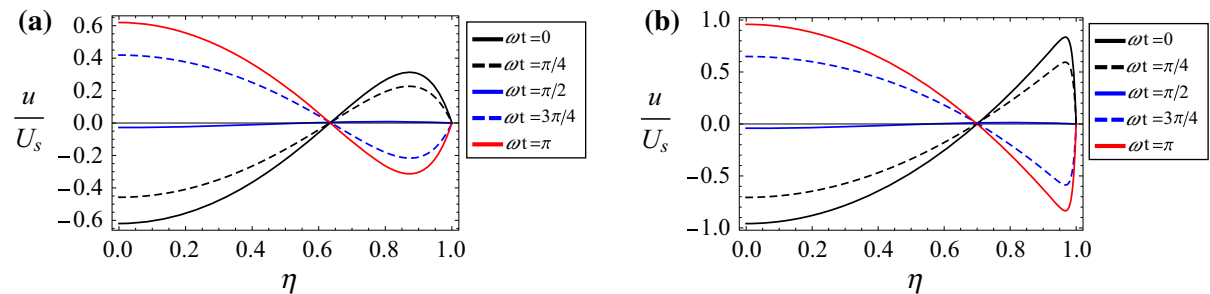


**Fig. 2** Scaled velocity distribution for the closed-ended tube, at different times during an oscillation cycle. **a**  $\alpha = 0.1$ ,  $\lambda = 10$ . **b**  $\alpha = 0.1$ ,  $\lambda = 100$

We begin by examining the properties of the EDL, as manifested through the distribution of the electric potential. The scaled potential,  $\Psi$ , obtained from a numerical solution of Eq. (1) and from the approximate solution (6), is plotted in Fig. 1. It may clearly be seen that for a lower surface potential, the approximate solution is virtually indistinguishable from the exact numerical solution; for high surface potentials, the approximation deviates and clearly over-predicts the exact solution. A value of  $\Psi_s = 4$  corresponds with a zeta potential of  $\psi_s \simeq -0.1$  V, which is considered to be a representative value [1]; Nevertheless, the approximate solution used in deriving the solutions for the velocity and concentration fields and, consequently, the dispersion coefficients, should be reasonably valid, particularly for large values of  $\lambda$ . Also noteworthy, the potential does not decay to zero when the ratio of the tube radius to the Debye length,  $\lambda < 7$ , in which case an overlapping of the EDLs may occur and the obtained solution may no longer be valid; in subsequent calculations, values of  $\lambda$  used will be chosen such that overlapping should not occur.

Next, the flow and concentration fields are examined, followed by their combined effect on the solute transport by an oscillating EOF within a closed-ended tube. This situation may be viewed as an approximate model of dead-end pores within a porous structure, where transport is generally limited to molecular diffusion alone; this often presents the bottleneck of processes such as catalysis and adsorption, which occur within such porous structures. For example, in packed beds of pelletised adsorbents, fluid induced mixing is effective in the intra-particle domain, where bulk flow may be driven by a pressure gradient. This pressure-driven mixing is ineffective when considering the inter-particle mass transfer. In such cases, applying an AC electric field will drive flow even in confined pores, and it is therefore of interest to examine the potential enhancement to the mass transfer within such dead-end pores.

As may be seen in Fig. 2, the flow under such conditions is essentially a superposition of an electro-osmotic flow, driven within the EDL, and a back-flow at the center of the tube, driven by the induced back-pressure. This velocity distribution becomes essentially parabolic, if the EDL is thin and  $\alpha \leq 1$ , save that the fluid adjacent to the wall flows in a direction opposite to that of the tube axis region. Increasing  $\alpha$  will alter this velocity distribution and



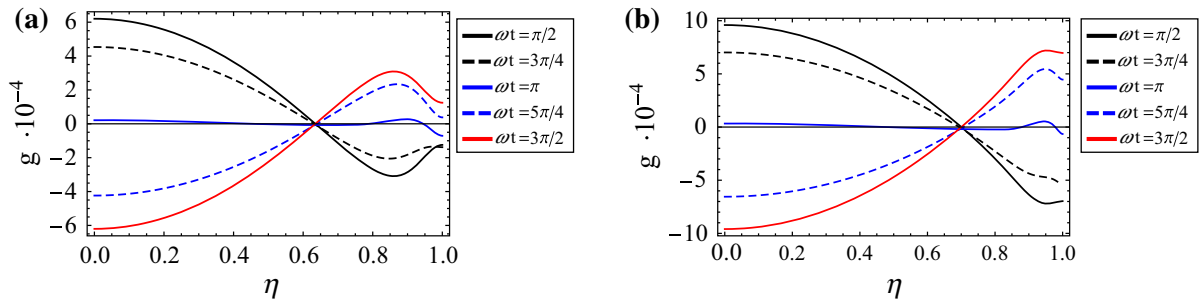


**Fig. 3** The function  $g$ , representing the scaled radial concentration distribution for the closed-ended tube, at different times during an oscillation cycle. **a**  $\alpha = 0.1, \lambda = 10$ . **b**  $\alpha = 0.1, \lambda = 100$ . Calculations made with  $Pe = 1$  and  $Sc = 1000$

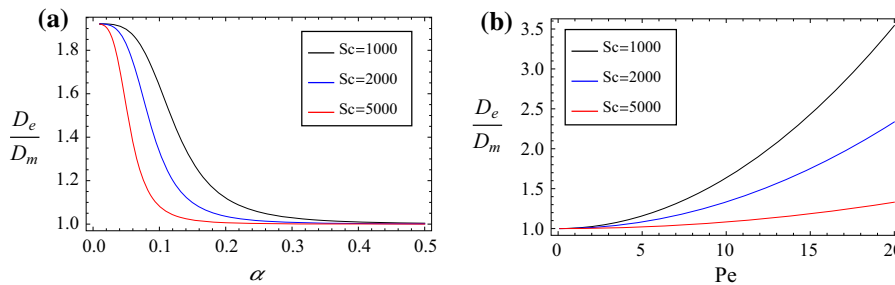


**Fig. 4** The variation of the dispersion coefficient and mass-transfer enhancement, represented by the ratio  $D_e/D_m$ , for various values of the Schmidt number,  $Sc$ . **a** As a function of the Womersley number,  $\alpha$ . **b** As a function of the Péclet number,  $Pe$ . Calculations made with  $\lambda = 100$

decrease the maximum velocity attainable. The concentration field (Fig. 3) shows considerably larger variations compared with a classical EOF in an open-ended tube, even for a low value of  $\alpha$ . This is a direct consequence of the back-flow; the low frequency limit is no longer a nearly uniform, plug-like flow outside the EDL, but a parabolic profile typical of laminar pressure-driven flow.

Since we are interested in mass-transfer enhancement within pores with small radii, there are two factors to consider before calculations of the dispersion coefficient are made. First, it is expected that the relevant values of  $\alpha$  will be correspondingly small, even for relatively high frequencies. This is particularly important since achieving a significant  $Pe$  at a high frequency may be difficult. Second, It may be plausible to consider the effect of relatively large EDL to pore radius ratios, say  $\lambda = 10$ .

Typical curves showing the variation of the dispersion coefficient with  $\alpha$  and  $Pe$ , for different  $Sc$ , are shown in Fig. 4. At a constant  $Pe$ , increasing the frequency results in a decreased maximum velocity attainable, which reduces the dispersion and level of mass-transfer enhancement. Another aspect is the fact that under a constant  $Pe$ , a slow diffuser exhibits a lower dispersion coefficient at higher frequencies; this is due to the fact that increasing the frequency leaves less time for the solute to diffuse in and out of the slower moving wall region of the velocity field, an essential part of the dispersion mechanism. A thicker EDL will also result in a lower dispersion coefficient, as illustrated in Fig. 5; this is due to the fact that, at a given applied electric field, the maximum velocity is lower in the presence of a thicker EDL.

Significant mass-transfer enhancement appears to be possible within the range of parameters employed. For example, in a pore with  $R = 1\mu\text{m}$ , applying a frequency of 400Hz corresponds with a value of  $\alpha = 0.05$ . For a solution with  $Sc = 1000$ , an electric field which results in a value of  $Pe = 20$  should be possible, resulting in a 300% increase in the mass-transfer rate. For a faster diffuser, the achievable Péclet number will be smaller, resulting in a lower degree of enhancement,  $\approx 20\%$  and  $\approx 80\%$  for  $Sc = 5000$  and  $Sc = 2000$ , respectively. For smaller pores, it would appear that only slow diffusing solutes may benefit from the enhanced mass transfer, under the considered constraints. As a final note, we consider that the mass-transfer efficiency can be viewed here as simply

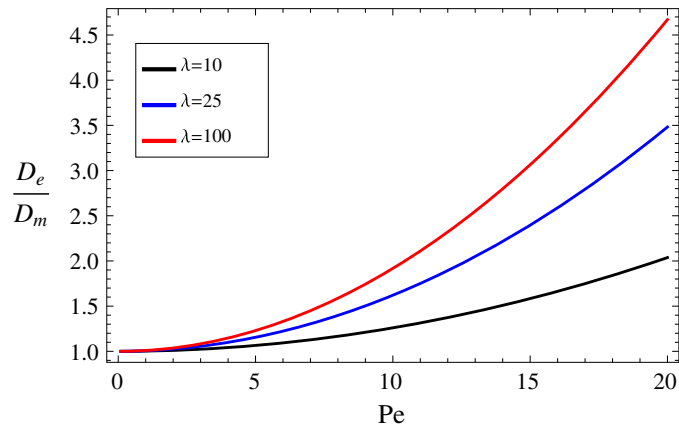


**Fig. 5** The variation of the mass-transfer enhancement, represented by the ratio  $D_e/D_m$ , as a function of  $Pe$ , for various values of  $\lambda$ . Calculations made for  $\alpha = 0.1$ ,  $Sc = 1000$

the ratio of dispersion to molecular diffusivity, which has been referred to in the forgoing sections as the degree of enhancement. Further, one may also estimate the power consumed,  $\mathcal{P} \approx U_s \rho_e E_0$ , the multiple of the velocity and the electric body force that generates it. We may scale the power against the Péclet number, as this quantity would then represent the power consumed per unit increase in dispersion effectiveness. Taking the charge density based on the average electric potential within the EDL, we find that  $\mathcal{P} \approx e \psi_s D_m E_0 / \lambda$ , which shows that the energetic efficiency of the electro-osmotic mass-transfer process increases when the EDL is thin (large  $\lambda$ ), and for a slow diffuser—for which  $Pe$  is high.

#### 4 Summary and conclusions

The foregoing analysis presented the time-averaged flux, represented by a dispersion coefficient, generated by an oscillating electro-osmotic flow in a closed-ended cylindrical tube. This configuration is envisioned as an approximate geometry for porous structures within pelletised, granular beds used, for example, for adsorption and catalysis. Within such pores, mass transfer is limited by diffusion and so enhancement of the transport rate is desirable. The calculated dispersion coefficient depends on the thickness of the electric double-layer relative to the pore size, as well as the solution properties and oscillation frequency—this is manifested by a parameter that represents the ratio of the diffusion and oscillation time-scales. At a given pore radius, the dispersion decreases with the frequency at a constant  $Pe$ , as has generally been observed for dispersion in oscillating flows; this is due to the reduced amplitude of the oscillatory motion. The effect of the scaled EDL thickness has been found to be of particular importance in determining the degree of mass-transfer enhancement, which appears to favour thin double layers. The results indicate that enhancement of mass transfer, due to time-averaged dispersion, is indeed possible under acceptable operating conditions, allowing, for example, up to a threefold enhancement in pores with a radius of  $1 \mu\text{m}$ . The ability to increase mass transfer within dead-end pores using an external stimuli may find use in nano/microfluidic devices, as well as applications where diffusion and chemical reactions occur within confined pores of a larger solid matrix, such as catalysis, adsorption and chromatography.

#### References

1. Probstein RF (2003) *Physicochemical hydrodynamics: an introduction*, 2nd edn. Wiley, New York
2. Stone HA, Stroock AD, Ajdari A (2004) Engineering flows in small devices: microfluidics toward a lab-on-a-chip. *Annu Rev Fluid Mech* 36:381–411
3. Squires TM, Quake SR (2005) Microfluidics: fluid physics at the nanoliter scale. *Rev Mod Phys* 77(3):977–1026

4. Kang Y, Yang C, Huang X (2002) Dynamic aspects of electroosmotic flow in a cylindrical microcapillary. *Int J Eng Sci* 40(20):2203–2221
5. Bhattacharya A, Masliyah JH, Yang J (2003) Oscillating laminar electrokinetic flow in infinitely extended circular microchannels. *J Colloid Interf Sci* 261:12–20
6. Erickson D, Li D (2003) Analysis of alternating current electroosmotic flows in a rectangular microchannel. *Langmuir* 19(13):5421–5430
7. Cussler EL (1997) *Diffusion: mass transfer in fluid systems*. Cambridge University Press, New York, p 580
8. Tallarek U, Vergeldt FJ, Van As H (1999) Stagnant mobile phase mass transfer in chromatographic media: intraparticle diffusion and exchange kinetics. *J Phys Chem B* 103:7654–7664
9. Forse AC, Gri JM, Merlet C, Carretero-Gonzalez J, Raji AO, Trease NM, Grey CP (2017) Direct observation of ion dynamics in supercapacitor electrodes using in situ diffusion NMR spectroscopy. *Nat Energy* 2:16216
10. Marcos Kang YJ, Ooi KT, Yang C, Wong TN (2005) Frequency-dependent velocity and vorticity fields of electro-osmotic flow in a closed-end cylindrical microchannel. *J Micromech Microeng* 15(2):301–312
11. Marcos Yang C, Ooi KT, Wong TN, Masliyah JH (2004) Frequency-dependent laminar electroosmotic flow in a closed-end rectangular microchannel. *J Colloid Interf Sci* 275(2):679–698
12. Zhang Y, Wong TN, Yang C, Ooi KT (2006) Dynamic aspects of electroosmotic flow. *Microfluid Nanofluid* 2(3):205–214
13. Huang HF, Lai CL (2006) Enhancement of mass transport and separation of species by oscillatory electroosmotic flows. *Proc R Soc A* 462:2017–2038
14. Ramon G, Agnon Y, Dosoretz C (2011) Solute dispersion in oscillating electro-osmotic flow with boundary mass exchange. *Microfluid Nanofluid* 10(1):97–106
15. Chatwin PC (1975) On the longitudinal dispersion of passive contaminant in oscillating flow in tubes. *J Fluid Mech* 71:513–527
16. Watson EJ (1983) Diffusion in oscillatory pipe flow. *J Fluid Mech* 133:233–244
17. Kurzweg UH (1985) Enhanced heat conduction in oscillating viscous flows within parallel-plate channels. *J Fluid Mech* 156:291–300